APPLIED PHYSICS LETTERS VOLUME 74, NUMBER 19 10 MAY 1999

Electrochemical deposition of nickel nanowire arrays in single-crystal mica films

L. Sun and P. C. Searson[a)]
Department of Materials Science and Engineering, The Johns Hopkins University, Baltimore, Maryland 21218

C. L. Chien
Department of Physics and Astronomy, The Johns Hopkins University, Baltimore, Maryland 21218

(Received 18 December 1998; accepted for publication 12 March 1999)

Nanopores with lateral dimensions as small as 30 nm have been fabricated by nuclear track etching in 5 μm thick, single-crystal muscovite mica wafers. The nanopores have a diamond shape with their axes aligned with the crystal axes of mica as a result of anisotropic etching. Nickel nanowire arrays have been fabricated by electrodeposition into the nanopores. The magnetic properties of the nanowire arrays are compared with those fabricated in polymer membranes. © *1999 American Institute of Physics.* [S0003-6951(99)04419-8]

Electrodeposition of metals into porous templates has been used as a method to fabricate quasi-one-dimensional metallic[1–5] and ferromagnetic[6–8] nanostructures. Anisotropic magnetic properties have been realized in both Ni and Co nanowires.[6–8] Subsequently, multilayered nanowires (e.g., Cu/Co) displaying giant magnetoresistance with current flow perpendicular to the interfaces have also been successfully fabricated.[9–11]

Templates for electrochemical deposition of nanowire arrays include etched nuclear particle tracks, porous alumina films formed by anodic oxidation of aluminum, and nanochannel glass. The properties of nanowire arrays are directly related to properties of the nanoporous template such as the relative pore orientations in the assembly, the pore size distribution, and the surface roughness of the pores. Most recent work has focused on nanowire arrays grown in polycarbonate membranes.[1–12] However, polymer membranes are not ideal since the internal surface of the pores can be quite rough.[13] Polymer membranes are also relatively soft so that characterization of the pore morphology is not straightforward. A further limitation associated with commercially available membranes is that the angle between the pore axis and the surface normal can be as high as 30°, which can greatly reduce the shape anisotropy.[8] Here we show that the coercivity and squareness of nickel nanowire arrays in mica films are significantly enhanced compared to nanowires of the same dimension grown in polycarbonate membranes.

Porous templates were fabricated by etching particle tracks in 5 μm thick single-crystal muscovite mica wafers (Spruce Pine Co). Particle tracks were created by exposure to $\approx$6 MeV α particles from a 100 μCi Cf^{252} source (Isotope Products) in a chamber at a pressure of about 10^{-3} Torr. The particle tracks were collimated to within 5° by locating the mica wafers 1.9 cm from the source. The track depth for 6 MeV α particles in mica was determined to be 9.7 μm, consistent with an energy deposition of 11–12 MeV cm^{-2} mg^{-1} for mica.[14]

The particle tracks were etched in 20 wt. % HF. The particle track etch rate and the lateral etch rate were determined from electrical conductance measurements[15,16] to be 1000 and 0.35 Å s^{-1}, respectively. From the ratio of the etch rates (2.86×10^3) the taper of the pore walls is determined to be 0.02°.

Nickel nanowire arrays were fabricated by electrochemical deposition into the mica templates. The electrode contact was provided by a sputter deposited gold layer. Nickel was deposited from a solution of $20\,g\,\ell^{-1}$ $NiCl_2\cdot6H_2O$, $515\,g\,\ell^{-1}$ $Ni(H_2NSO_3)_2\cdot4H_2O$, $20\,g\,\ell^{-1}$ H_3BO_3 buffered to pH 3.4 at a potential of -1.0 V (Ag/AgCl).[6]

Figure 1 shows a scanning electron microscope (SEM) image of an irradiated and etched mica film sectioned to reveal the interior of the pores. It is evident that the pore axes are parallel, and that the interior surfaces of the pores are smooth, clean, and free from etching residues. The pores are diamond shaped with well defined corners indicating that the etching of mica in HF is highly anisotropic.[17]

Figure 2 shows a 2 μm$\times$2 μm atomic force microscope (AFM) image of the surface of a mica film with 50 nm pores illustrating that the nanopores have the same shape, size, and orientation. They are randomly distributed in two dimensions with a density of 1×10^9 cm^{-2}. Images from both sides of

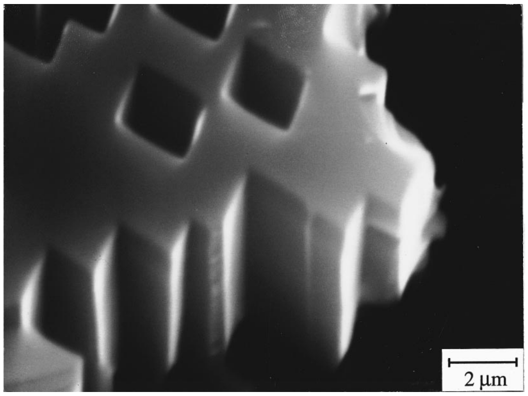

FIG. 1. Scanning electron microscope image of 2.3 μm pores in single-crystal mica.

[a)]Electronic mail: searson@jhu.edu

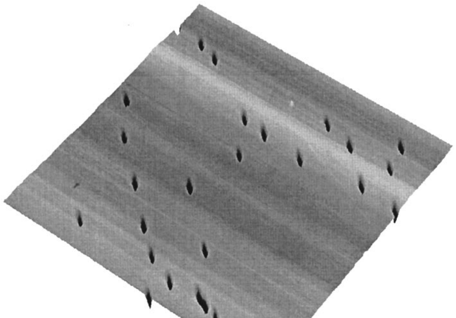

FIG. 2. 2 μm×2 μm AFM image showing 50 nm pores in a single-crystal mica film.

the mica wafers after etching were identical, with no observable differences in pore size, pore density, pore shape, and orientation. The diamond shaped pores are well defined, independent of size, and are characterized by angles of 60° and 120°. We use an effective diameter to characterize the pore size, defined as the diameter of a circle having the same area as the diamond.

The shape of the pores in the mica films is due to the anisotropy in the in-plane etch rates, originating from the crystal structure of the mica. X-ray diffraction patterns obtained from mica powder prepared by grinding the wafers confirmed the monoclinic structure with the expected lattice parameters ($a_1 = 5.18$ Å, $a_2 = 9.02$ Å, $a_3 = 10.02$ Å, $\alpha = \gamma = 90°$, $\beta = 95.5°$).[18–20] X-ray $\theta/2\theta$ diffraction of the single-crystal mica wafers revealed only the $(00n)$ peaks, indicating that the cleavage surface is the (001) plane. The (001) cleavage plane has a rectangular structure with in-plane lattice vectors a_1 and a_2. By measuring the angular dependence of the projections of diffraction vectors which are tilted from the surface normal with an angle ψ, we can determine the orientations of the in-plane lattice vectors in reciprocal space b_1 and b_2. For the monoclinic mica lattice we have $a_1 \| b_1$ and $a_2 \| b_2$. Thus by comparing the lattice vectors with images of the pores, we can determine the crystal orientation of the pore walls.

Figure 3(a) shows ϕ scans for the {112}, $\{\bar{1}\bar{1}2\}$, and {023} planes. For the monoclinic structure of mica, the (112) and $(1\bar{1}2)$, $(\bar{1}12)$ and $(\bar{1}\bar{1}2)$, (023) and $(0\bar{2}3)$ planes have the same 2θ and ψ values. Furthermore, the in-plane projections of these planes are very close to the [1 1 0], $[1\,\bar{1}\,0]$, $[\bar{1}\,1\,0]$, $[\bar{1}\,\bar{1}\,0]$, [0 1 0], and $[0\,\bar{1}\,0]$ directions in reciprocal space. Comparison of the lattice vectors with images of the surface reveals that the pore walls are parallel to the {110} planes in the mica lattice, as shown in Fig. 3(b). The pore walls correspond to the oxygen terminated planes, indicating that these are the slowest etching planes, very similar to the etching process in SiO_2. The 60° angle of the diamond-shaped pores determined from SEM and AFM images is very close to the angle of 59.7° of the diamond enclosed by $a_1 = 5.18$ Å and $a_2 = 9.02$ Å.

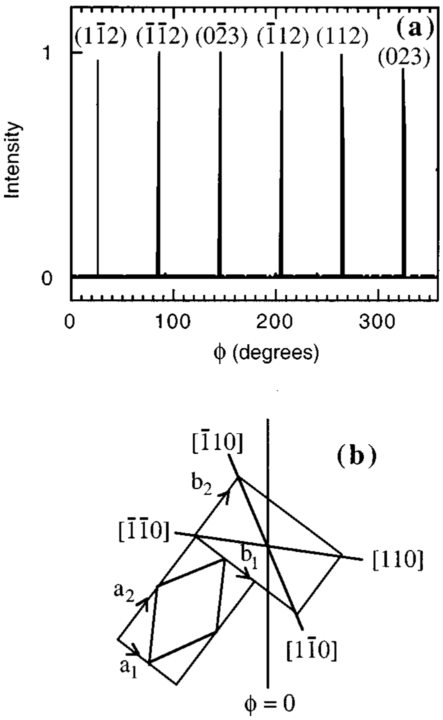

FIG. 3. (a) X-ray ϕ scans of {112}, $\{\overline{1\,1}\,2\}$, and {023} peaks of mica single-crystal film. (b) Lattice vectors (a_1 and a_2), reciprocal lattice vectors (b_1 and b_2), and reciprocal vectors $[\overline{1\,1}\,0]$, $[\bar{1}\,1\,0]$, [1 1 0], and $[1\,\bar{1}\,0]$.

Arrays of nickel nanowires with effective diameters from 30 to 200 nm were fabricated by electrochemical deposition into mica templates. In order to maintain approximately the same volume of nickel in the films, the nanowire density was increased from 5×10^7 cm^{-2} for the 200 nm pores to 2×10^9 cm^{-2} for the 30 nm pores. The relevant parameters are shown in Table I. A disadvantage of the relatively high volume fractions necessary for magnetic measurements is an increase in the number of overlapping pores. Table I shows the calculated fraction of double and triple pores.[16,21] From the table it can be seen that the fraction of double pores is expected to be about 4% and the fraction of triple pores about 0.1%. It is important to minimize the fraction of double and triple pores since their larger effective diameter may significantly reduce any property enhance-

TABLE I. Effective diameter d, number density of tracks n, and area (volume) fraction f of pores, $m(1)/n$, $m(2)/n$, and $m(3)/n$ represent the calculated fraction of pores derived from single, double, and triple tracks.

d (nm)	n (No. cm^{-2})	f	$m(1)/n$	$m(2)/n$	$m(3)/n$
200	5×10^7	0.0157	0.939	0.0295	0.000 617
150	1×10^8	0.0177	0.932	0.0330	0.000 776
100	3×10^8	0.0236	0.910	0.0429	0.001 35
75	5×10^8	0.0221	0.915	0.0404	0.001 19
50	1×10^9	0.0196	0.925	0.0363	0.000 950
30	2×10^9	0.0141	0.945	0.0267	0.000 504

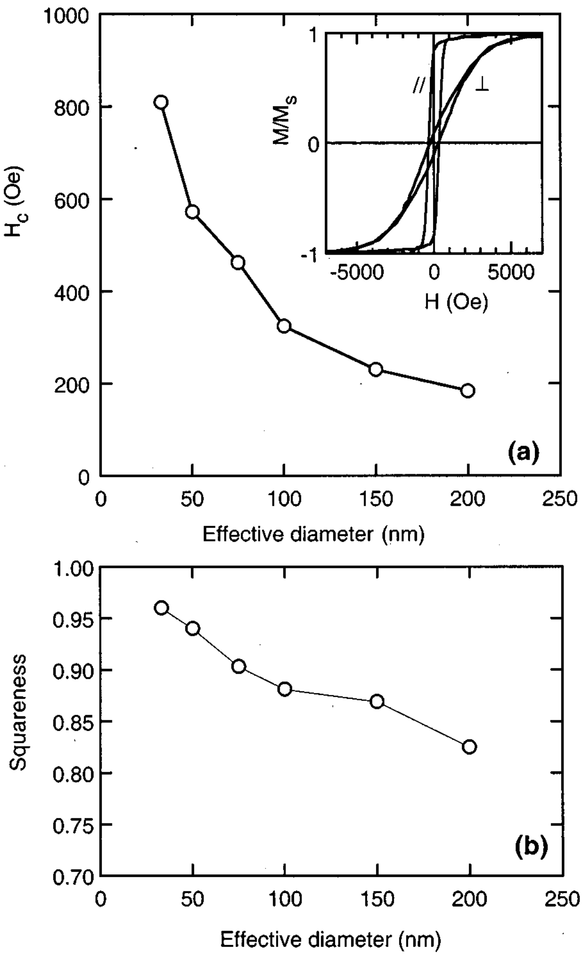

FIG. 4. (a) Coercivity and (b) squareness of nickel nanowire arrays in single-crystal mica films as a function of the effective wire diameter. The inset in (a) shows typical hysteresis curves for a nickel nanowire array with an effective pore diameter of 100 nm obtained with the magnetic field applied parallel (‖) and perpendicular (⊥) to the wire axes.

ments (e.g., coercivity, squareness) associated with the smaller pores.

The hysteresis loops for the Ni nanowire arrays exhibited strong shape anisotropy due to the nanowire geometry, as shown in the inset of Fig. 3. The easy directions are along the wire axes, whereas the hard axes are perpendicular to the wires with a saturation field, due to the demagnetization factor, of $2\pi M = 3.0\,\text{kOe}$ at room temperature.

Figure 4(a) shows the size dependence of the coercivity H_c as a function of the effective wire diameter with the field applied parallel to the wires (perpendicular to the film). The measured coercivity increases with decreasing effective diameter, reaching a value of 800 Oe at an effective wire diameter of 30 nm. For smaller diameters, coercivities in excess of 1 kOe can be readily anticipated. These values are slightly larger than previous results for nickel nanowire arrays in polycarbonate membranes,[6] suggesting that the improved collimation and lower surface roughness of the pore surface play an important role in determining the properties of the nanowires.

Figure 4(b) shows the magnitude of the remanent magnetization obtained from the hysteresis loops and plotted as the squareness (SQ), defined as the ratio of remanence and saturation magnetization $(\mathrm{SQ}=M_r/M_s)$. The value of SQ is as high as 0.96 for the 30 nm diam wires, decreasing gradually to 0.83 for the 200 nm diam wires. The maximum value of 0.96 is significantly larger than the value of 0.90 obtained for 30 nm diam wires in polycarbonate membranes.[6–8] Furthermore, the value of 0.83 for the 200 nm diam wires is more than a factor of 2 larger than the value of 0.3 obtained for 200 nm wires in polycarbonate membranes. These enhancements can be attributed directly to the improved collimation of the pores, the uniform pore cross section, and the low density of overlapping pores.

[1] G. E. Possin, Rev. Sci. Instrum. **41**, 772 (1970).
[2] G. E. Possin, Physica (Utrecht) **55**, 339 (1971).
[3] W. D. Williams and N. Giordano, Rev. Sci. Instrum. **55**, 410 (1984).
[4] J. T. Madsen and N. Giordano, Phys. Rev. B **31**, 6395 (1985).
[5] C. R. Martin, Science **266**, 1961 (1994).
[6] T. M. Whitney, J. S. Jiang, P. C. Searson, and C. L. Chien, Science **261**, 1316 (1993).
[7] L. Piraux, S. Dubois, E. Ferain, R. Legras, K. Ounadjela, J. M. George, J. L. Maurice, and A. Fert, J. Magn. Magn. Mater. **165**, 352 (1997).
[8] R. Ferre, K. Ounadjela, J. M. George, L. Piraux, and S. Dubois, Phys. Rev. B **56**, 14066 (1997).
[9] L. Piraux, J. M. George, J. F. Despres, C. Leroy, E. Ferain, R. Legras, K. Ounadjela, and A. Fert, Appl. Phys. Lett. **65**, 2484 (1994).
[10] A. Blondel, J. P. Meier, B. Boudin, and J.-Ph. Ansermet, Appl. Phys. Lett. **65**, 3019 (1994).
[11] K. Liu, K. Nagodawithana, P. C. Searson, and C. L. Chien, Phys. Rev. B **57**, 7381 (1995).
[12] S. K. Chakarvarti and J. Vetter, Nucl. Instrum. Methods Phys. Res. B **62**, 109 (1991).
[13] G. Guillot and F. Rondelez, J. Appl. Phys. **52**, 7155 (1981).
[14] A. Sigrist and R. Balzer, Radiat. Eff. **34**, 75 (1977).
[15] C. P. Bean, M. V. Doyle, and G. Entine, J. Appl. Phys. **41**, 1454 (1970).
[16] J. A. Quinn, J. L. Anderson, W. S. Ho, and W. J. Petzny, Biophys. J. **12**, 990 (1972).
[17] H. A. Khan, N. A. Khan, and R. Spohr, Nucl. Instrum. Methods **189**, 577 (1981).
[18] W. W. Jackson and J. West, Zeit. F. Krist. **76**, 211 (1930).
[19] W. W. Jackson and J. West, Zeit. F. Krist. **85**, 160 (1933).
[20] W. L. Bragg, *Atomic Structure of Minerals* (Cornell University Press, New York, 1937).
[21] The fraction of overlapping pores was calculated from the approximation: $m(q)/n=(4f)^{q-1}/q![1-4f+8f^2-(32/3)f^3+\ldots]$, where $m(q)$ is the number of pores derived from q particle tracks, n is the track density, f is the area fraction of pores assuming all single pores.